

# Three-Dimensional Numerical Studies on the Effect of the Particle Charge to Mass Ratio Distribution in the Electrostatic Coating Process

N. Toljic\*, K. Adamiak, *Fellow IEEE*, G. S. P. Castle, *Life Fellow IEEE*, Hong-Hsiang (Harry) Kuo and Hua-Tzu (Charles) Fan

Department of Electrical and Computer Engineering  
University of Western Ontario  
phone: 1 519 661 2111  
e-mail: ntoljic@uwo.ca

**Abstract**--Charge to mass ratio is a crucial parameter that governs the behavior of particle trajectories in a charged cloud of particles. The complex nature of the charging process limits our ability to accurately determine the charging level when particles of varying size are present. Using a numerical approach, it is possible, however, to take into account predefined values for this parameter. In this paper, the average charge to mass ratio and the distribution of the charge to mass ratio in the coating of a flat target were systematically varied to demonstrate their effect on the motion of the charged particles. The results show that the transfer efficiency increases as the average charge to mass ratio increases. It was found that the transfer efficiency is a weak function of the average particle size in the range tested and that it increases as the width of the size distribution increases.

## I INTRODUCTION

Much theoretical and experimental research has been devoted to assess the value of charge to mass ratio ( $q/m$ ) of individual particles in a charged particle population, when they are electrically charged by induction or conduction. However, the complex nature of the charging process limits our ability to make definite conclusions. Using a numerical approach, however, it is possible to study the effects of different values of charging level and distribution of charge on particle trajectories and deposition efficiency.

All the measurement techniques for particle charge can be classified in two major groups: static and dynamic [1-2]. In the static methods particle charge is measured directly, whereas in the dynamic methods it is calculated indirectly from the measurement of the particle mobility. Static methods are crude and simple, but they can be easily implemented. Dynamic methods are more reliable, but they introduce significant complexity in the system. It has been shown in [2] that considerable conflicting data exists for the dependence of  $q/m$  on particle size and suggested that this area needs further experimental and theoretical research.

A number of published papers describe methods and report results for the numerical simulation of the charged particle motion using FLUENT. In [3], numerical modeling of a complete powder coating process was carried out to understand the gas-particle two-phase flow field inside a powder coating booth and the results of the numerical simulation were compared with experimental data to validate the numerical model. In this previous study,  $q/m$  was considered to be constant for all sizes of the particles. In [4], FLUENT was used to solve the mechanical portion of the spraying process and the user defined functions were used to solve the Poisson equation governing the electric field distribution. The  $q/m$  was the same for all the particles since the particles were practically monodispersed. Ye et al. [5] presented the results of investigations aiming to numerically simulate the electrostatic powder coating process. They used the assumption that the  $q/m$  changes inversely to particle radius. The assumption of the inverse relation between  $q/m$  and the particle radius was also used by Colbert [6]. So far, however, there has been no systematic approach to examine the effects of the  $q/m$  distribution on the particle trajectories and deposition efficiency.

In this paper, the average charge to mass ratio ( $Q/M$ ) and the distribution of the  $q/m$  in a particle population were systematically varied to demonstrate their effects on the motion of the charged particles. It has been assumed that the particle  $q/m$  varies with the particle radius:

$$\frac{q}{m} = Ar^n \quad (1.1)$$

where  $q$  is the particle charge,  $m$  is the particle mass,  $r$  is the particle radius and  $A$  and  $n$  are unknown coefficients. The aim of this study is to numerically examine and quantify the importance of the unknown coefficients  $A$  and  $n$ .

In the subsequent sections, a typical industrial coating process is simulated. The mechanical phenomena are modeled with the computational fluid dynamics software FLUENT. Custom user-defined functions are used to solve the Poisson field by incorporating it into the general scalar transport equations within FLUENT. This enables the calculation of the electrostatic force on the charged particles. Coupling between the airflow phase, the particle discrete phase and the electrostatic field yields the trajectories of the charged particles.

## II THEORETICAL CONSIDERATIONS

Particles can acquire charge through tribo, corona, conduction or induction charging phenomena. Tribo charging refers to the process in which two different materials contact and separate, leaving both materials charged to the same magnitude but with different polarity. This process can be explained using the concepts of Fermi level and work function. The material with higher affinity for electrons gains electrons (i.e., lower Fermi level or higher work function) and charges negatively, while the material with lower affinity (i.e., higher Fermi level or lower work function) loses electrons and charges positively. In corona charging, particles subjected to the stream of ions can become charged by ionic attachment onto the surface of the individual particles. Conduction charging refers to a process in which neutral solid or liquid particles are in electrical contact with an electrode, supplied with high voltage. Charge flows from the voltage supply to the material surface due to the presence of the electric field formed between the voltage supply and the adjacent ground. In the separation process, particles retain charge. Induction charging refers to a process in which a voltage is connected to an electrode which is placed adjacent to the grounded material undergoing atomization. Electric charge flows from the ground to the material surface due to the induced electric field and becomes trapped on the particle when it separates from ground.

Contradictory data were reported in published papers regarding the dependency of charge to radius. Namely, charge can be considered to be linearly dependent of particle radius, particle surface or particle volume. This results in three possible values of the parameter  $n$ .

### A. $n=-2$

If we assume that the particle charge varies linearly with particle radius then  $q/m$  is inversely proportional to the square of particle radius:

$$\frac{q}{m} \sim \frac{r}{\rho V} \sim \frac{1}{r^2} \quad (2.1)$$

where  $\rho$  is the particle density and  $V$  is its volume.

### B. $n=-1$

If we assume that the particle surface charge density is constant then  $q/m$  is inversely proportional to the particle radius:

$$\frac{q}{m} \sim \frac{S}{\rho V} \sim \frac{1}{r} \quad (2.2)$$

where  $S$  is the particle surface area.

### C. $n=0$

If we assume that the particle volume charge is constant then  $q/m$  is independent of particle radius:

$$\frac{q}{m} \sim \frac{V}{\rho V} \neq f(r) \quad (2.3)$$

In the following sections, the effects of each of these dependencies on the particle deposition pattern are examined, assuming a simplified coating system with a rotary bell atomizer and a flat target.

## III COMPUTATIONAL DOMAIN AND NUMERICAL PROCEDURES

The three-dimensional computational domain encompasses a simplified model of the electrostatic rotary bell atomizer and a flat target of the radius 0.5m situated 0.25m away from the atomizer (Figure 1).

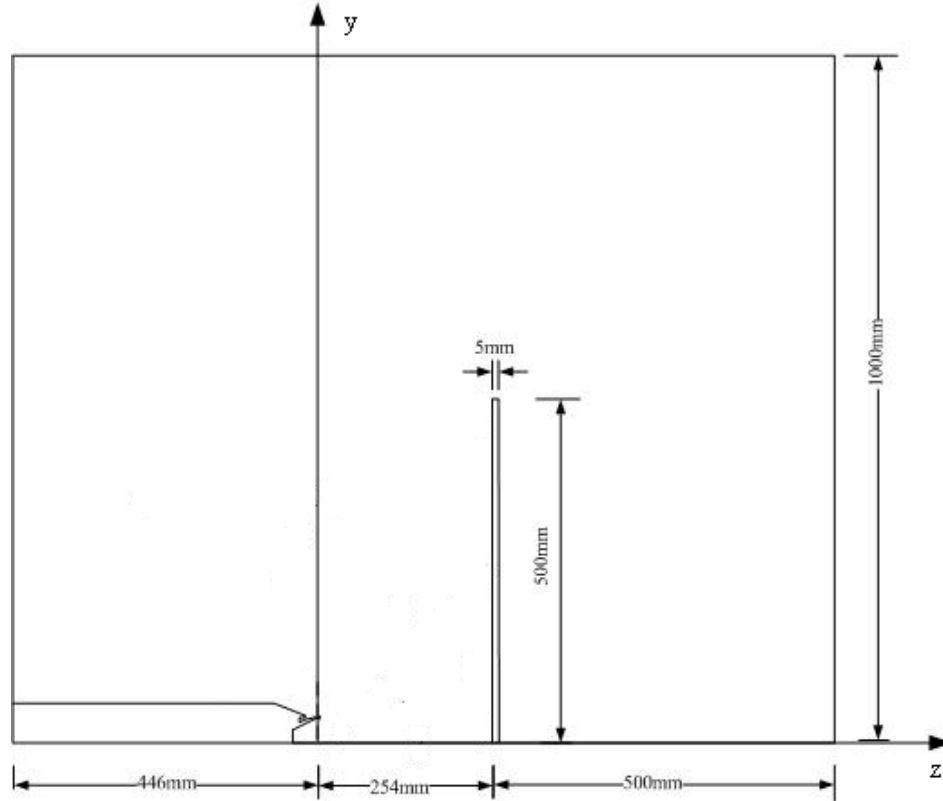


**Figure 1: Computational domain of the investigated coating system consisting of a rotary bell atomizer and a flat circular target**

The computational domain is a box, 1200mm in length, 1000mm in width and 1000mm in height. The shaping air flows out of the atomizer through a ring-shaped slit 1mm in width. The particles are ejected from the edge of the atomizer. The width of the atomizer edge is assumed to be 0.5mm. The geometry of the computational domain was created by the GAMBIT software package [7] and meshed with hexagonal and tetrahedral cells in an unstructured manner. The mesh between the atomizer and the target was refined compared to the rest of the computational domain. The numerical algorithm includes solving the gas phase of the shaping air, the discrete phase of the charged particles, the electrostatic field and coupling between them to get a self-consistent solution [4].

The shaping air flow in FLUENT was considered as incompressible, steady, viscous and turbulent. The RNG (renormalization group)  $k-\varepsilon$  turbulent model was used in the modeling. The particle discrete phase in FLUENT is solved using the Lagrangian approach in which the particles are traced by the stochastic tracking (random walk) model in turbulent gas flow [8]. Coupling between the air flow and the particle discrete phase is included via source terms of mass and momentum. The particles are ejected with the predefined size and charge distribution and directed by the shaping air to the target.

The electric field generated by the voltage applied to the bell cup and the space charge formed by the charged particles is governed by Poisson's equation

$$\nabla^2 \Phi = -\frac{\rho}{\varepsilon_0} \quad (3.1)$$

where  $\Phi$  is the electrical potential,  $\rho$  is the space charge density and  $\varepsilon_0$  is the permittivity of the air. The electric field intensity  $\mathbf{E}$  can be calculated as

$$\mathbf{E} = -\nabla \Phi \quad (3.2)$$

The Poisson's equation can be solved within FLUENT using the user-defined scalar transport equations [9]. The diffusion coefficient and the source term in the FLUENT transport equation are substituted with the electrical permittivity and the space charge density, respectively. The space charge density in a cell can be calculated as

$$\rho = \frac{1}{N} \sum_{i=1}^N q_i / m_i \cdot C_i \quad (3.3)$$

where  $q_i, m_i, C_i$  are the total charge, mass and concentration of the particles of the given size in the cell, and  $N$  is the total number of particle sizes.

#### IV NUMERICAL RESULTS AND DISCUSSION

In order to examine the effect of the  $q/m$  distribution, a number of numerical simulations were carried out. The shaping air flow rate was set to be 0.02 kg/s. The atomizer voltage was set to be -90kV and the target was grounded. The value of the  $q/m$  was varied in a systematic manner, while the values of the other input parameters were kept constant. Numerical results were classified in four groups. The first group describes the effects of the  $Q/M$ . The second group describes the effects of  $q/m$  to radius dependency. The third and the fourth groups deal with the average particle size effects and the effects of the width of the size distribution, respectively. The base values for the particle size distribution and the corresponding mass flow rates are given in Table 1. These data were obtained experimentally.

| Particle diameter[ $\mu\text{m}$ ] | 10   | 15   | 20   | 25  | 30   | 35  | 40   | 45    | 50   | 55   | 60   | 65    | 70    | 75   | 80    |
|------------------------------------|------|------|------|-----|------|-----|------|-------|------|------|------|-------|-------|------|-------|
| Flow rate[g/s]                     | 0.03 | 0.15 | 0.36 | 0.6 | 0.84 | 0.9 | 0.81 | 0.588 | 0.45 | 0.39 | 0.24 | 0.186 | 0.168 | 0.15 | 0.138 |

**Table 1: Parameters of the size distribution**

A bar chart of the size distribution is depicted in Figure 2.

For all the cases, transfer efficiency is calculated as a ratio of the input flow rate and the deposition mass flow rate. Input flow rate is the controlled parameter and the deposition mass flow rate is calculated by FLUENT internally.

##### A. Effect of the $Q/M$

To examine the effect of the  $Q/M$ , numerical simulations with low, medium and high value of the  $Q/M$  were carried out. For simplicity, the radius exponent,  $n$  is chosen to be zero, i.e.  $Q/M$  is constant with size. Parameter  $A$  from the equation (1.1) is chosen so that the low, medium and high values of  $Q/M$  are set to 0.5mC/kg, 1mC/kg and 2mC/kg, respectively. The corresponding numerical results for the deposition profiles along the radius of the target are depicted in the Figure 3.

The accumulation rate in the regions around the centre of the target is practically zero. This is attributed to the mechanical forces of the shaping air which on the target have only a radial component in the outwards direction. As the radial position is increased, the accumulation rate increases, reaches its maximum and then gradually decreases to almost zero value at the edge of the target. The maximum value of the accumulation rate increases as the  $Q/M$  increases. The transfer efficiencies for  $Q/M$  equal to 0.5mC/kg, 1mC/kg and 2mC/kg are 93.1%, 96% and 97.9%, respectively. This shows that the transfer efficiency increases as the  $Q/M$  increases. This can be explained by the increased magnitude of the electrostatic forces between the particles and the target.

##### B. Effect of the $q/m$ to Radius Dependency

To examine the effects of the  $q/m$  radius dependency, numerical simulations were conducted with radius exponent equal to 0, -1 and -2. The  $Q/M$  for all the cases is 1mC/kg. The numerical results for the deposition profile along the radius of the target are depicted in the Figure 4.

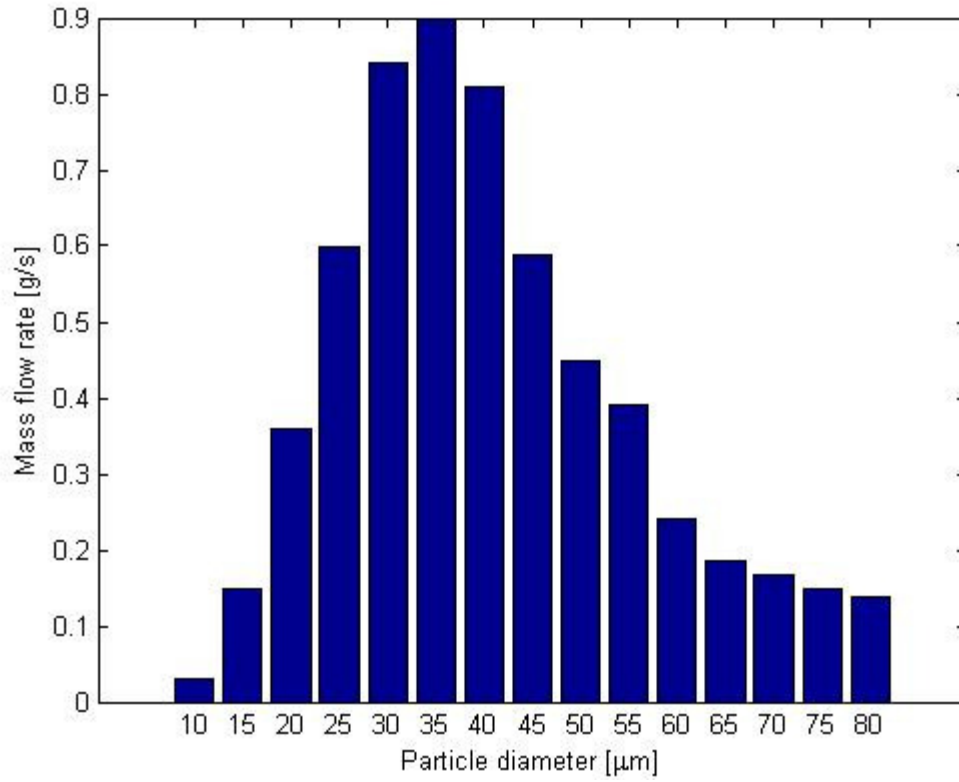


Figure 2: Bar chart of the particle size distribution

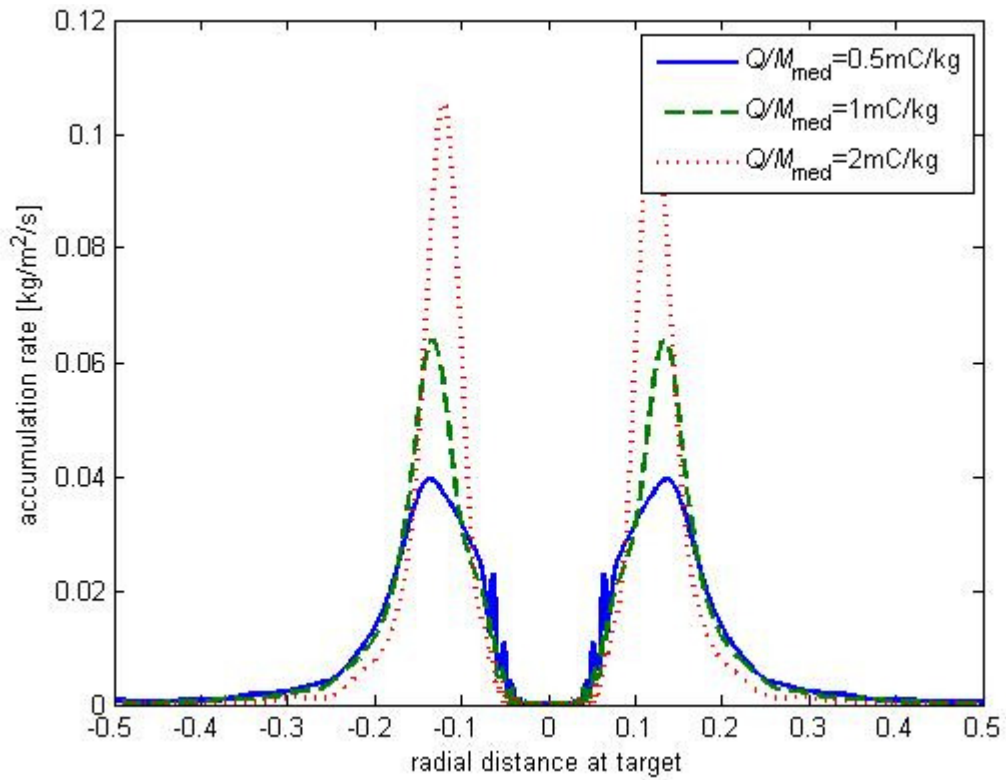
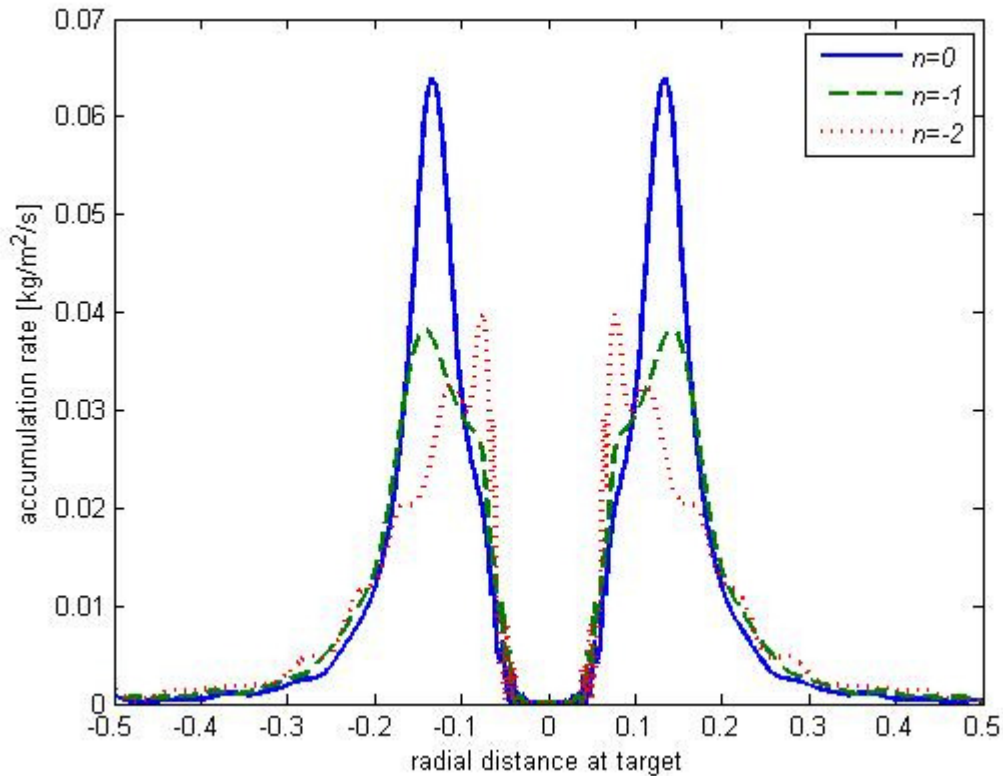


Figure 3: Accumulation rate along the target surface for different values of the average  $Q/M$



**Figure 4: Accumulation rate along the target surface for different values of parameter  $n$**

The deposition pattern becomes more uniform as the radius exponent increases in magnitude. The transfer efficiencies for particle radius exponent equal to 0, -1 and -2 are 96%, 92.9% and 87.4%, respectively.

The general shape of the graph resembles the one in the previous case. Again, we have zero accumulation around the centre of the target, a sharp increase and then gradual decrease of the accumulation rate as the radial position is increased. It can be noted that the transfer efficiency decreases as the magnitude of radius exponent increases. This can be explained by the fact that under these conditions the larger particles carry less charge. With regards to distribution, the charged cloud expands because of the mutual repulsion of the charged particles and this makes the particles distribute more uniformly on the target surface.

### *C. Effect of the median particle size*

To examine the effect of the median particle size, numerical simulations were conducted with average particle diameter set to 25 $\mu\text{m}$ , 35 $\mu\text{m}$  and 45 $\mu\text{m}$ . The size distribution for the case with the average particle size set to 35 $\mu\text{m}$  is given in the Table 1. The size distributions for cases with the average particle size set to 25 $\mu\text{m}$  and 45 $\mu\text{m}$  are derived from the values in Table 1 by decreasing or increasing the values in the first row by 10 $\mu\text{m}$ . The  $Q/M$  for all the cases is 1mC/kg and the radius exponent from the equation (1.1) is -1. The corresponding numerical results for deposition profile along the radius of the target are depicted in the Figure 5.

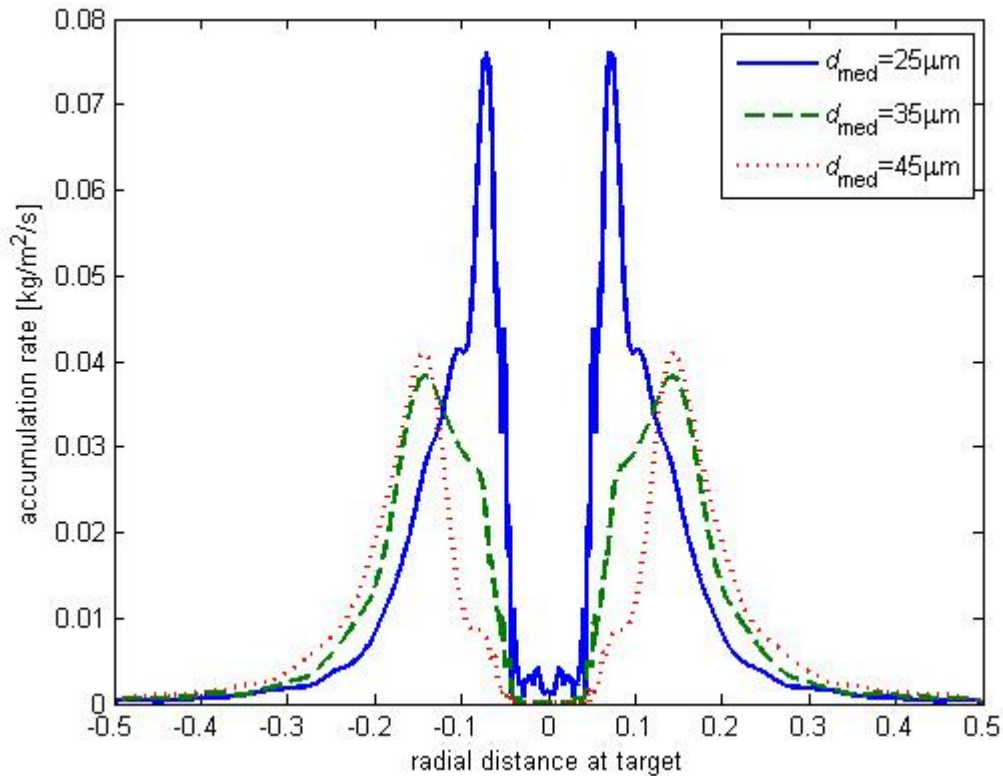


Figure 5: Accumulation rate for different values of the average particle size

The transfer efficiencies for the average particle size equal to 25 $\mu\text{m}$ , 35 $\mu\text{m}$  and 45 $\mu\text{m}$  are 91.2%, 93% and 92.6% respectively.

It can be noted that the transfer efficiency is a weak function of the average particle size. For the median value of the average particle size the transfer efficiency curve exhibits a weak local maximum. However, the relative difference between the transfer efficiency values for the three different sub-cases can also be a result of the numerical error introduced by the software used. For the larger values of the average particle size, there are more larger particles which carry higher values of charge, repel under the influence of the electric forces and deposit more uniformly at the target. Note that the mass fraction of the smaller particles is relatively low. Also, because the assumed value of  $q/m$  for particles with 17.5 $\mu\text{m}$  radius is equal in all the cases, the larger value of volume average particle radius will result in lower  $Q/M$  and vice versa.

#### D. Effect of the width of the size distribution

To examine the effect of the width of the size distribution, numerical simulations were conducted with monodispersed and polydispersed particles. The monodispersed case contains only one injection stream with particle diameter set to 35 $\mu\text{m}$  and the corresponding mass flow rate set to 0.006kg/s. The polydispersed case follows data given in Table 1. The  $Q/M$  for all the cases is 1mC/kg and the radius exponent from the equation (1.1) for the wide distribution is -1. The corresponding numerical results for deposition profile are depicted in Figure 6.

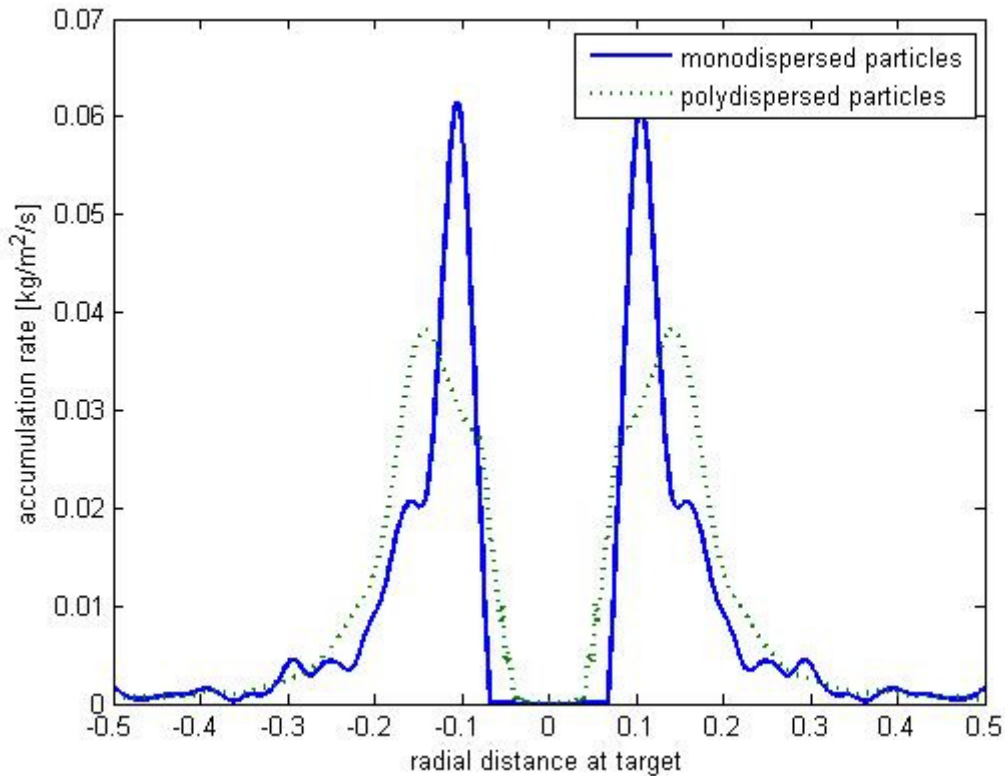


Figure 6: Accumulation rate for different size distribution widths

The transfer efficiencies for the monodispersed case and polydispersed case with normal size distribution are 84.3% and 92.9%, respectively. It can be noted that the transfer efficiency increases as the width of the size distribution increases. The local maximum of the accumulation rate for the monodispersed case is greater than the local maximum of the accumulation rate for the polydispersed case. The larger particles that are present in the case of wide size distribution carry more charge and significantly increase transfer efficiency. The charged cloud expands because of the mutual repulsion of the charged particles and this makes the particles distribute more uniformly on the target surface.

#### V CONCLUSION

In this paper, the charge-to-mass average value and its distribution in the particle population were systematically varied to demonstrate their effects on the motion and deposition of the charged particles. In order to do so, a typical industrial coating process was simulated. The mechanical part was modeled with the commercial computational fluid dynamics software, FLUENT. Its user-defined functions were used to solve the Poisson field by incorporating it into the general scalar transport equations within FLUENT. Coupling between the airflow phase, the particle discrete phase and the electrostatic field yields the trajectories of the charged particles. The numerical results show that the transfer efficiency increases as the  $Q/M$  increases, which can be explained by the increased value of the electrostatic forces between the particles and the target. The charged cloud expands because of the mutual repulsion of the charged particles and this makes the particles distribute more uniformly on the target surface. It was also noted that the transfer efficiency decreases as the radius exponent increases. This can be explained by the fact that the smaller particles are more likely to be repelled by the space charge cloud, if the values of charge they carry is higher and this condition is fulfilled for the smaller values of the radius exponent. It can be noted that the transfer efficiency is a weak function of the average particle size. The lower values of the average particle size result in the lower overall charge that the particles carry and in the lower transfer efficiency. The transfer efficiency increases as the width of the size distribution increases. The smaller particles that are present in the case of wide size distribution are more easily controlled by the electric forces which results in increased transfer efficiency.

## REFERENCES

- [1] R. C. Brown, "Tutorial review: Simultaneous measurement of particle size and particle charge", *J. Aerosol Sci.*, vol. 98, pp. 1373–1391, 1997.
- [2] N. Toljic, K. Adamiak and G. S. P. Castle, "Determination of particle charge to mass ratio distribution in electrostatic applications: A brief review", *Proc. ESA Annual Meeting on Electrostatics*, Minneapolis, Minnesota, June 2008.
- [3] U. Shah, J. Zhu, C. Zhang, F. Wang and R. Martinuzzi "Validation of a numerical model for the simulation of an electrostatic powder coating process", *Int. J. of Multiphase Flow*, Vol. 33, Issue 5, pp. 557-573, May 2007.
- [4] S. Zhao, K. Adamiak and G.S.P. Castle, "The implementation of Poisson field analysis within FLUENT to model electrostatic liquid spraying", *2007 IEEE Canadian Conference on Electrical and Computer Engineering*, Vancouver, Apr. 22-25, 2007.
- [5] Q. Ye and J. Domnick, "On the simulation of space charge in electrostatic powder coating with a corona spray gun", *Powder Technol.* 135–136, pp. 250–260, 2003
- [6] S. Colbert," Numerical simulations of droplet trajectories from an electrostatic rotary-bell atomizer", Doctoral Dissertation, Drexel University, 2007.
- [7] GAMBIT 6.2 User's Guide, FLUENT Inc., 2005.
- [8] FLUENT 6.2 User's Guide, FLUENT Inc., 2005.
- [9] FLUENT 6.2 UDF Manual, FLUENT Inc., 2005.